International Journal of Thermofluid Science and Technology (2022)
Volume 9, Issue 5, Paper No. 090501
https://doi.org/10.36963/IJTST.2022090501

Research Article

Investigation of air and rice husk cold flow structures in the suspension furnace chamber through a simulation study

Soen Steven[1], Linda Windari[1], Novebriantika Novebriantika[1], Pasymi Pasymi[2], Elvi Restiawaty[1,3], Yazid Bindar[*,1,3]

[1] *Department of Chemical Engineering, Faculty of Industrial Technology, Institut Teknologi Bandung, Jl. Ganesha 10, Bandung, 40132, Indonesia*
[2] *Department of Chemical Engineering, Faculty of Industrial Technology, Universitas Bung Hatta, Padang, Indonesia*
[3] *Department of Bioenergy Engineering and Chemurgy, Faculty of Industrial Technology, Institut Teknologi Bandung, Jl. Ganesha 10, Bandung, 40132, Indonesia*

ARTICLE INFO

Received: 22 May 2022;
Received in revised form:
28 July 2022;
Accepted: 06 July 2022;
Published online:
12 Aug. 2022

Keywords:
Suspension furnace
Turbulent
Reynold stress model
Multiphase flow
Swirl

ABSTRACT

Rice husk combustion in the suspension furnace is not an easy matter. Until now, there are still many obstacles faced in its process as characterized by low combustion conversion. The main cause is the poor air-particle contact as well as the probability of particle elutriation out of the furnace chamber before combustion completely occurs. Thus, in-depth and detailed understanding of air and rice husk cold flow structures in the furnace chamber, as proposed in this study, becomes necessary. The simulation study was conducted using Reynold stress model (RSM) for fluid flow quantification whereas discrete phase model was utilized for particle flow quantification. The simulation results reveal that cylindrical chamber gives a more significant particle residence time rather than rectangular chamber for every similar excess air amount. Besides, providing burner with a tangential air inlet of 90^{o} results in high turbulence, intense swirl phenomenon, and long particle residence time. Moreover, the furnace chamber equipped with a smaller burner diameter and longer burner length together will augment the air-particle contact in the furnace chamber. Despite providing the best condition for the furnace, the design must not forget to consider the economical aspect.

1. Introduction

As time passes, the research on biomass utilization for fuel or chemicals purposes is frequently conducted for its environmentally friendly [1–6]. Indonesia has abundant rice husk availability, as agricultural biomass, for it is the 3rd largest rice producer in the world after China and India [7]. The rice production was around 44.6 MT/y in 1990, then continued to increase to 66.4 MT/y in 2010, and almost reached 80 MT/y in 2016 [8]. Due to the tremendous production of rice, the by-product in the form of rice husk is also greatly

[*]*Corresponding e-mail*: ybybyb@fti.itb.ac.id (Yazid Bindar)

produced since it occupies an average value of 20%-wt [9–11].

Until now, however, rice husk utilization is still low and rare because of no nutritional value [12,13]. It is manifested by rice husk which is only destroyed through opened and uncontrolled burning or at least only used as growth mediums, briquettes, or animal feeds [14–16]. In contrast, rice husk has a significant heating value and ash content compared to other agricultural biomass [17–19]. The silica content in ash also occupies as much as 87-97%-wt which becomes green and sustainable resources for silica production through rice husk combustion and followed by ash extraction [20–23].

The studies of rice husk combustion have been widely performed either in muffle furnaces [24], torch furnaces [25], fluidized bed furnaces [26], or suspension furnaces [13,27,28]. Under all of those furnaces, the high degree of rice husk combustion conversion is reflected by perfect air and particle contact [29]. It is strongly influenced by combustion air amount, air providing technique, raw material physicochemical properties, burner geometry, and furnace chamber type [11,13,19,30,31]. However, those factors aforementioned are often unintentionally overlooked since the difficulties in scrutinizing the multiphase phenomena of air and particle contact through direct experimental study [32–35]. Thus, the cold flow structure simulation between air and rice husk (in absence of combustion phenomena) becomes the alternative study to carry out [36]. With the ability to examine air and rice husk cold flow structure in the furnace, air-particle contact that is difficult to research can be clearly revealed using computational fluid dynamics (CFD) method [37–39].

Nowadays, the CFD study becomes cheap, established, and powerful tool to improve the rice husk combustion process performance [40]. In consequence, complete and efficient combustion can expectedly be achieved [41–43]. Moreover, the application of CFD in the biomass thermal conversion process can accurately predict the process in terms of hydrodynamics, combustion product distribution, temperature distribution, ash deposit behavior, and even CO and NO_X emissions [44–47]. Still, CFD can identify the particle elutriation phenomena under air flow fields [48] which also contributed to the high carbon content in biomass combustion products. Interestingly, a lot of works with regard to cold flow modelling of air and particle are conducted in cyclones, hydrocyclones, or pipes [42,49–52] but are still scarce for furnace chambers.

The CFD study by Pasymi et al. (2017) on the tangential burner informs that flow structure is not only influenced by tangential inlet conditions but also by initial tangential intensity and air amount [53]. Meanwhile, Dinh et al. (2017) stated the enhancement of inlet air amount greatly impacts perfect mixing and high heat transfer rate in such a way as to homogenize the temperature distribution and lead to the completeness of combustion [54]. In addition, the other studies on gas-solid hydrodynamics are employed for evaluating baffled fluidized bed reactor [55] or contactor column with corrugated structure packing [56]. According to Gungor and Yildirim (2013), the furnace equipped with excellent air-particle mixing and contact is able to result in high reaction rates and consequently could acquire satisfying combustion conversion [57].

The simulation study on multiphase hydrodynamics phenomena of air and rice husk in the suspension furnace chamber is still rarely reported. This study, accordingly, intends to disclose it. Besides revealing the air and rice husk flow structures in the furnace chamber, this study is also aimed to examine the influences of furnace chamber geometries, excess air amount, and burner configurations on air-particle contact (represented by particle residence time). The intended burner configurations comprise tangential air inlet angle, burner diameter, and burner length. Under all these parameters, the air and rice husk flow structures and particle residence time become the scrutinized variables.

2. Materials and methods

2.1 Geometry design and meshing

The suspension furnace consists of the axial air inlet, tangential air inlet, rice husk

inlet, burner, secondary air inlet, furnace chamber, and outlet. Its geometry and dimensions are shown in Figures 1a-b. Subsequently, the type of grid was chosen as a structured quadrilateral. The grid independence test was carried out under several conditions, i.e. very coarse (with a grid number of 300,000), coarse (with a grid number of 520,000), medium (with a grid number of 1,000,000), fine (with a grid number of 1,800,000), and very fine (with a grid number of 2,000,000). The meshing technique was also aided by inflation at near wall area with the element size of 15 mm. Figure 1c is associated with the meshing result under medium grid number. The inputted properties, as well as various variables, followed Table 1.

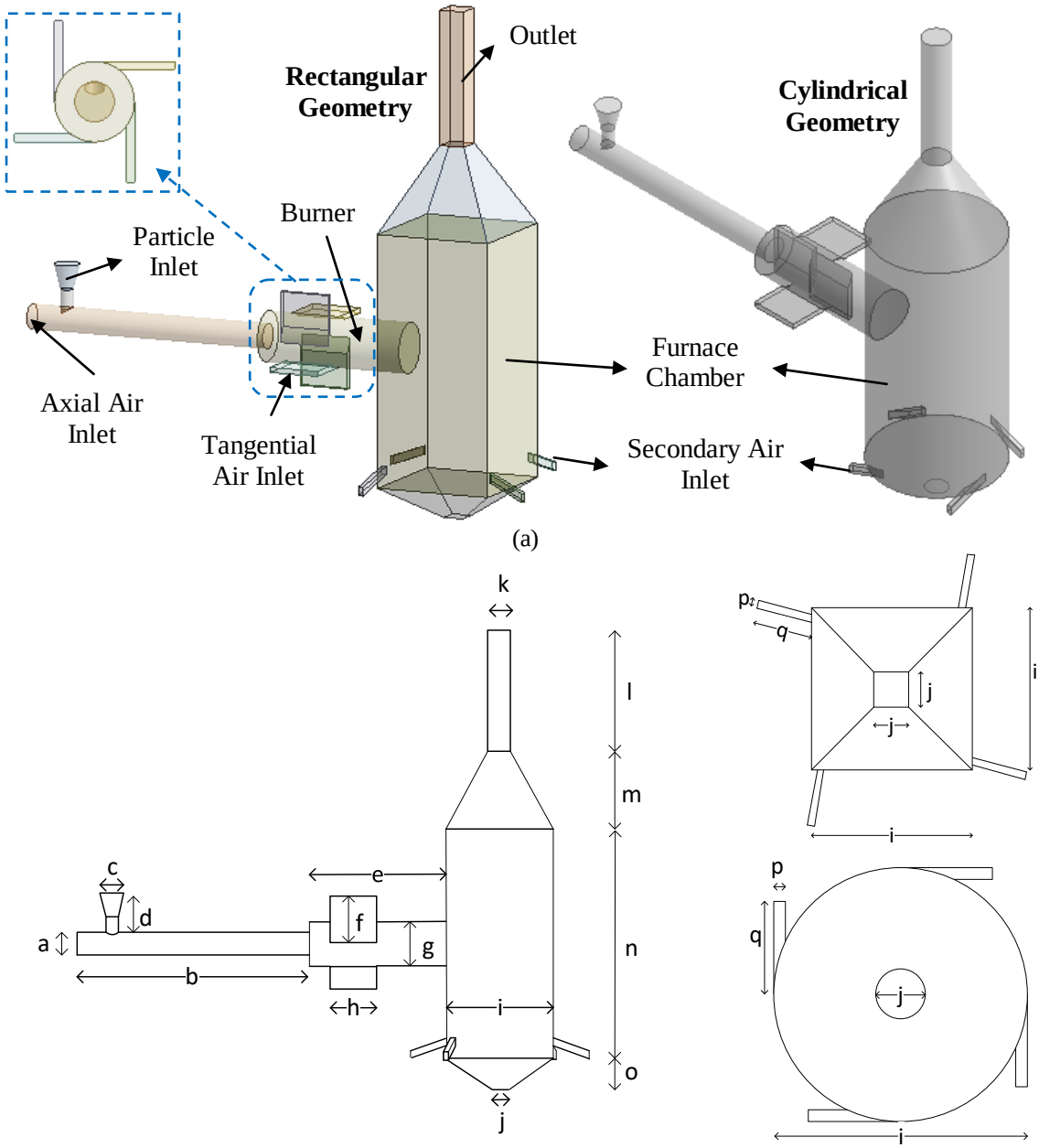

a=149 mm; d=278 mm; g=300 mm; j=120 mm; m=500 mm; p=50 mm;
b=1500 mm; e=900 mm; h=300 mm; k=150 mm; n=1500 mm; q=300 mm
c=150 mm; f=300 mm; i=700 mm; l=800 mm; o=200 mm;

(b)

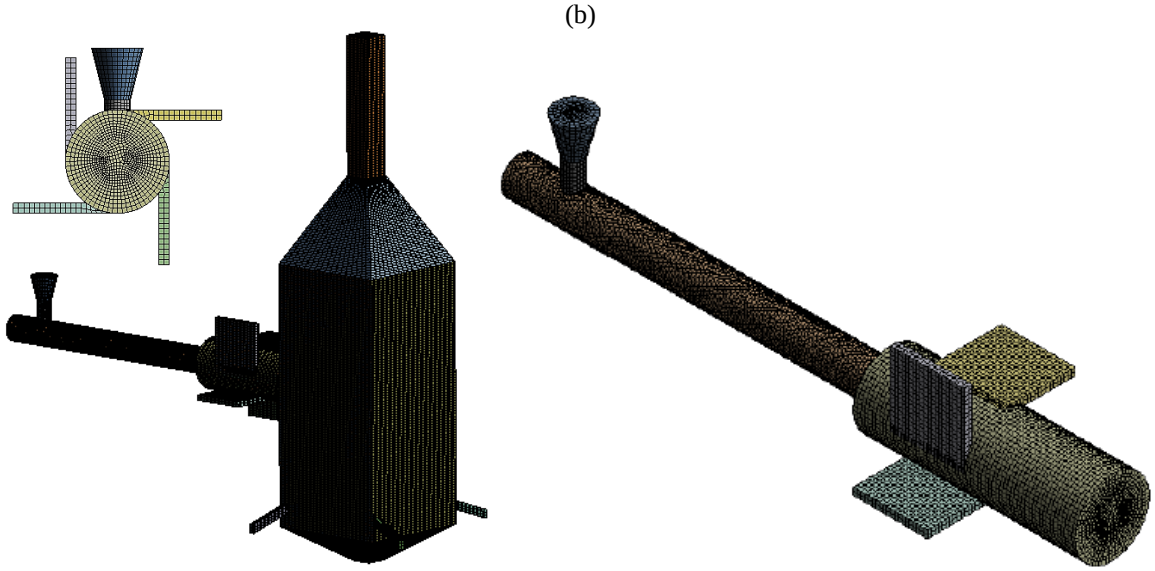

(c)

Figure 1. Suspension furnace geometry (a); Dimensions (b); and Meshing result under medium grid number (c)

Table 1. Properties, geometries, and operation conditions

Parameters	Values	Units
Air density	1.225	kg/m^3
Air viscosity	1.789×10^{-5}	kg/m/s
Rice husk particle density	650	kg/m^3
Rice husk particle diameter	0.03	cm
Rice husk particle sphericity	0.2	-
Rice husk loading rate	51.2	kg/h
Secondary to primary air ratio	7/3	-
Furnace chamber geometry	Rectangular, Cylindrical	-
Excess air (EA)	80, 110, 140, 170 200	%
Tangential air inlet angle	20, 45, 60, 90	^{o}
Burner diameter	30, 40, 50, 70	cm
Burner length	60, 90, 120, 150, 180, 210	cm

2.2 Mathematical formula of the turbulent model

The turbulent model used to solve the problems is the Reynold stress model (RSM) because it is known to be able to model flow with the attendance of swirl [58]. Each component of the Reynold stress ($\overline{\rho u_i' u_j'}$, later is expressed as R_{ij}) follows the law of conservation with the transport equation is written in equation 1. It has transient term ($\frac{\partial R_{ij}}{\partial t}$), convection term (C_{ij}), molecular diffusion term ($D_{L,ij}$), turbulent diffusion term ($D_{T,ij}$), Reynold stress production term (P_{ij}), production term (G_{ij}), stress term by pressure (ϕ_{ij}), and Reynold stress dissipation term (ε_{ij}) [43]. Pressure stress term involves the damping effect ($\phi_{ij,w}$) for locations close to the wall. This equation also involves the Reynold stress near the wall R_{lm}, R_{il}, and R_{jl}. The term n_l is the l component that is perpendicular to the wall while d is the distance to the wall. The constant values for RSM are $C_1 = 1.8$, $C_2 = 0.6$, $C_1' = 0.5$, $C_2' = 0.3$, $C_3 = 0.392$, $\sigma_R = 0.82$, and $C_\mu = 0.09$ [59].

$$\frac{\partial R_{ij}}{\partial t} + C_{ij} = D_{L,ij} + D_{T,ij} + P_{ij} - G_{ij} + \phi_{ij} - \varepsilon_{ij} \quad (1a)$$

$$C_{ij} = \sum_{l=x}^{y,z} \frac{\partial}{\partial l}\left(\bar{u}_l\, R_{ij}\right) \quad (1b)$$

$$D_{L,ij} = \sum_{l=x}^{y,z} \frac{\partial}{\partial l}\left[\frac{\mu}{\rho}\frac{\partial R_{ij}}{\partial l}\right] \quad (1c)$$

$$D_{T,ij} = \sum_{l=x}^{y,z} \frac{\partial}{\partial l}\left[\frac{\mu_t}{\sigma_R\,\rho}\frac{\partial R_{ij}}{\partial l}\right] \quad (1d)$$

$$P_{ij} = -\left(R_{ix}\frac{\partial \bar{u}_j}{\partial x} + R_{jx}\frac{\partial \bar{u}_i}{\partial x}\right) - \left(R_{iy}\frac{\partial \bar{u}_j}{\partial y} + R_{jy}\frac{\partial \bar{u}_i}{\partial y}\right) - \left(R_{iz}\frac{\partial \bar{u}_j}{\partial z} + R_{jz}\frac{\partial \bar{u}_i}{\partial z}\right) \quad (1e)$$

$$G_{ij} = -\frac{\mu_t}{\rho N_{prt}}\left(g_i\frac{\partial \rho}{\partial j} + g_j\frac{\partial \rho}{\partial i}\right) \quad (1f)$$

$$\phi_{ij} = \phi_{ij,1} + \phi_{ij,2} + \phi_{ij,w} \quad (1g)$$

$$\phi_{ij,1} = C_1\frac{\varepsilon}{k}\left(R_{ij} - \frac{2}{3}\delta_{ij}\rho k\right) \quad (1h)$$

$$\phi_{ij,2} = -C_2\left\{P_{ij} + G_{ij} - C_{ij} - \frac{2}{3}\delta_{ij}0.5(P+G-C)\right\} \quad (1i)$$

$$\phi_{ij,w} = C_1{}'\frac{\varepsilon}{\rho k}\left\{R_{lm}n_l n_m\delta_{ij} - \frac{3}{2}R_{il}n_j n_l - \frac{3}{2}R_{jl}n_i n_l\right\}C_3\frac{k^{\frac{3}{2}}}{\varepsilon d} + C_2{}'\frac{\varepsilon}{k}\left\{\phi_{lm,2}n_l n_m\delta_{ij} - 32\phi il,2njnl - 32\phi jl,2ninlC3k32\varepsilon d\right. \quad (1j)$$

$$P = \frac{1}{2}\left(P_{xx} + P_{yy} + P_{zz}\right) \quad (1k)$$

$$G = \frac{1}{2}\left(G_{xx} + G_{yy} + G_{zz}\right) \quad (1l)$$

$$C = \frac{1}{2}\left(C_{xx} + C_{yy} + C_{zz}\right) \quad (1m)$$

$$\varepsilon_{ij} = \frac{2}{3}\delta_{ij}\rho\varepsilon \quad (1n)$$

The turbulent kinetic energy k in the RSM equation is served in equation 2. On the other hand, the turbulent energy dissipation rate ε is modelled in the form of the transport equation as given in equation 3. The calculation of turbulent energy dissipation rate needs a constant $C_{\varepsilon 3}$ (stated in equation 3a) which is evaluated from the velocity component parallel to the direction of gravity ($u_{\parallel g}$) and the velocity component perpendicular to the gravity ($u_{\perp g}$). Afterward, the turbulent viscosity is computed from equation 4.

$$\rho\frac{\partial k}{\partial t} + \rho\bar{u}_x\frac{\partial k}{\partial x} + \rho\bar{u}_y\frac{\partial k}{\partial y} + \rho\bar{u}_z\frac{\partial k}{\partial z} = \frac{\partial}{\partial x}\left[\left(\mu + \frac{\mu_t}{\sigma_k}\right)\frac{\partial k}{\partial x}\right] + \frac{\partial}{\partial y}\left[\left(\mu + \frac{\mu_t}{\sigma_k}\right)\frac{\partial k}{\partial y}\right] + \frac{\partial}{\partial z}\left[\left(\mu + \frac{\mu_t}{\sigma_k}\right)\frac{\partial k}{\partial z}\right] + \frac{1}{2}\left(P_{xx} + P_{yy} + P_{zz}\right) + \frac{1}{2}\left(G_{xx} + G_{yy} + G_{zz}\right) \quad (2)$$

$$\rho\frac{\partial \varepsilon}{\partial t} + \rho\bar{u}_x\frac{\partial \varepsilon}{\partial x} + \rho\bar{u}_y\frac{\partial \varepsilon}{\partial y} + \rho\bar{u}_z\frac{\partial \varepsilon}{\partial z} = \frac{\partial}{\partial x}\left[\left(\mu + \frac{\mu_t}{\sigma_\varepsilon}\right)\frac{\partial \varepsilon}{\partial x}\right] + \frac{\partial}{\partial y}\left[\left(\mu + \frac{\mu_t}{\sigma_\varepsilon}\right)\frac{\partial \varepsilon}{\partial y}\right] + \frac{\partial}{\partial z}\left[\left(\mu + \frac{\mu_t}{\sigma_\varepsilon}\right)\frac{\partial \varepsilon}{\partial z}\right] + C_{\varepsilon 1}\frac{1}{2}\frac{\varepsilon}{k}\left[P_{xx} + P_{yy} + P_{zz} + C_{\varepsilon 3}\left(G_{xx} + G_{yy} + G_{zz}\right)\right] - C_{\varepsilon 2}\,\rho\frac{\varepsilon^2}{k} \quad (3)$$

$$C_{\varepsilon 3} = \frac{exp\left(\frac{u_{\parallel g}}{u_{\perp g}}\right) - exp\left(-\frac{u_{\parallel g}}{u_{\perp g}}\right)}{exp\left(\frac{u_{\parallel g}}{u_{\perp g}}\right) + exp\left(-\frac{u_{\parallel g}}{u_{\perp g}}\right)} \quad (3a)$$

$$\mu_t = C_\mu\rho\frac{k^2}{\varepsilon} \quad (4)$$

The rice husk flow is quantified by the discrete phase model where the particle has a velocity field that is controlled by the momentum balance of each particle [33,60]. Particle interacts with fluid through friction force which is formulated through the particle drag equation. For each particle with diameter of d_p, the particle velocity field has components $\bar{u}_{px}$, $\bar{u}_{py}$, and $\bar{u}_{pz}$. The equation for the conservation of momentum of a particle

is expressed in equations 5a-c. The contact time between the particle and fluid at every coordinate, namely t_{Dx}, t_{Dy}, and t_{Dz}, is formulated in equations 6a-c. Meanwhile, equations 7a-e indicate the friction coefficient (C_D) is the function of the spherical diameter (φ_p) [61,62].

$$\frac{\partial \bar{u}_{px}}{\partial t} = \frac{\bar{u}_x - \bar{u}_{px}}{t_{Dx}} + \frac{\rho_p - \rho}{\rho_p} g_x + a_x \quad (5a)$$

$$\frac{\partial \bar{u}_{py}}{\partial t} = \frac{\bar{u}_y - \bar{u}_{py}}{t_{Dy}} + \frac{\rho_p - \rho}{\rho_p} g_y + a_y \quad (5b)$$

$$\frac{\partial \bar{u}_{pz}}{\partial t} = \frac{\bar{u}_z - \bar{u}_{pz}}{t_{Dz}} + \frac{\rho_p - \rho}{\rho_p} g_z + a_z \quad (5c)$$

$$t_{Dx} = \frac{\rho_p d_p^2}{18\mu} \frac{24}{C_D N_{Rep,x}} \quad with \ N_{Rep,x} = \frac{\rho d_p (\bar{u}_x - \bar{u}_{px})}{\mu} \quad (6a)$$

$$t_{Dy} = \frac{\rho_p d_p^2}{18\mu} \frac{24}{C_D N_{Rep,y}} \quad with \ N_{Rep,y} = \frac{\rho d_p (\bar{u}_y - \bar{u}_{py})}{\mu} \quad (6b)$$

$$t_{Dz} = \frac{\rho_p d_p^2}{18\mu} \frac{24}{C_D N_{Rep,z}} \quad with \ N_{Rep,z} = \frac{\rho d_p (\bar{u}_z - \bar{u}_{pz})}{\mu} \quad (6c)$$

$$C_D = \frac{\beta_1 N_{Rep}}{\beta_2 + N_{Rep}} + \frac{24}{N_{Rep}} \left(1 + \beta_3 N_{Rep}^{\beta_4}\right) \quad (7a)$$

$$\beta_1 = exp(4.905 - 13.894\,\varphi_p + 18.422\,\varphi_p^2 - 10.260\,\varphi_p^3) \quad (7b)$$

$$\beta_2 = exp(1.468 + 12.258\,\varphi_p - 20.732\,\varphi_p^2 + 15.885\,\varphi_p^3) \quad (7c)$$

$$\beta_3 = exp(2.329 - 6.458\,\varphi_p + 2.449\,\varphi_p^2) \quad (7d)$$

$$\beta_4 = 0.096 + 0.556\,\varphi_p \quad (7e)$$

where a_x, a_y, a_z are three-dimensional acceleration of the external force.

2.3 Simulation setup

The simulation was in steady-state mode and was conducted using ANSYS Fluent 2021. It used default solution methods for pressure and absolute solution methods for velocity. The wall was set stationary under no-slip conditions which means zero speed on the wall surface. The wall function used in this study was standard wall function since it is widely applied in CFD for industrial flow analysis [59]. Subsequently, the SIMPLEC algorithm was selected for pressure velocity coupling with the spatial discretization methods as outlined in Table 2. Other than that, the relaxation factors were set at 0.3 for pressure stress, 1 for density, 1 for body forces, 0.7 for momentum, 0.8 for turbulent kinetic energy, 0.8 for turbulent dissipation rate, 1 for turbulent viscosity, and 0.5 for Reynold stresses. The convergence criteria for all variables were 10^{-6} and the calculation was held for 1000 iterations.

Table 2. Spatial discretization solving scheme

Variables	Scheme
Pressure (p)	PRESTO
Momentum (u_x, u_y, u_z)	QUICK
Turbulent kinetic energy (k)	Second Order Upwind
Turbulent dissipation rate (ε)	Second Order Upwind
Reynold stress (R_{ij})	First Order Upwind

3. Results and discussion

3.1 Turbulent model validation and grid independence test result

The turbulent model was first validated by the experimental study of cyclonic turbulent flow by Hoekstra (1999) [63]. His study is chosen with the consideration of geometry which is relatively clear, simple, easy to imitate, and has complete information. The cyclone was a 2D2D type (Figure 2a) which has main diameter of 29 cm, overall height of 116 cm, and cone height of 72.5 cm. The base

of the cyclone was 10.8 cm in diameter, the vortex finder was 14.5 cm in diameter, 29 cm in height, and was submerged halfway into the main cyclone body. The inlet was flat with height of 14.5 cm and width of 5.8 cm, turbulent intensity of 10%, and the ratio of length scale and cyclone diameter of 0.7. The particle density was 2740 kg/m^3. The tangential air inlet of the cyclone was introduced at a Reynold number of 280,000. Air velocity in his experiment was measured using a laser doppler anemometry (LDA) instrument. The validation was carried out by comparing tangential velocity data from the experiment and CFD simulation on various turbulent models (RSM, k-ε, and k-ω). Tangential velocity data was measured at the radial position of z = 65 cm, z = 40 cm, and z = 30 cm. The comparison results are plotted in Figures 2b-d.

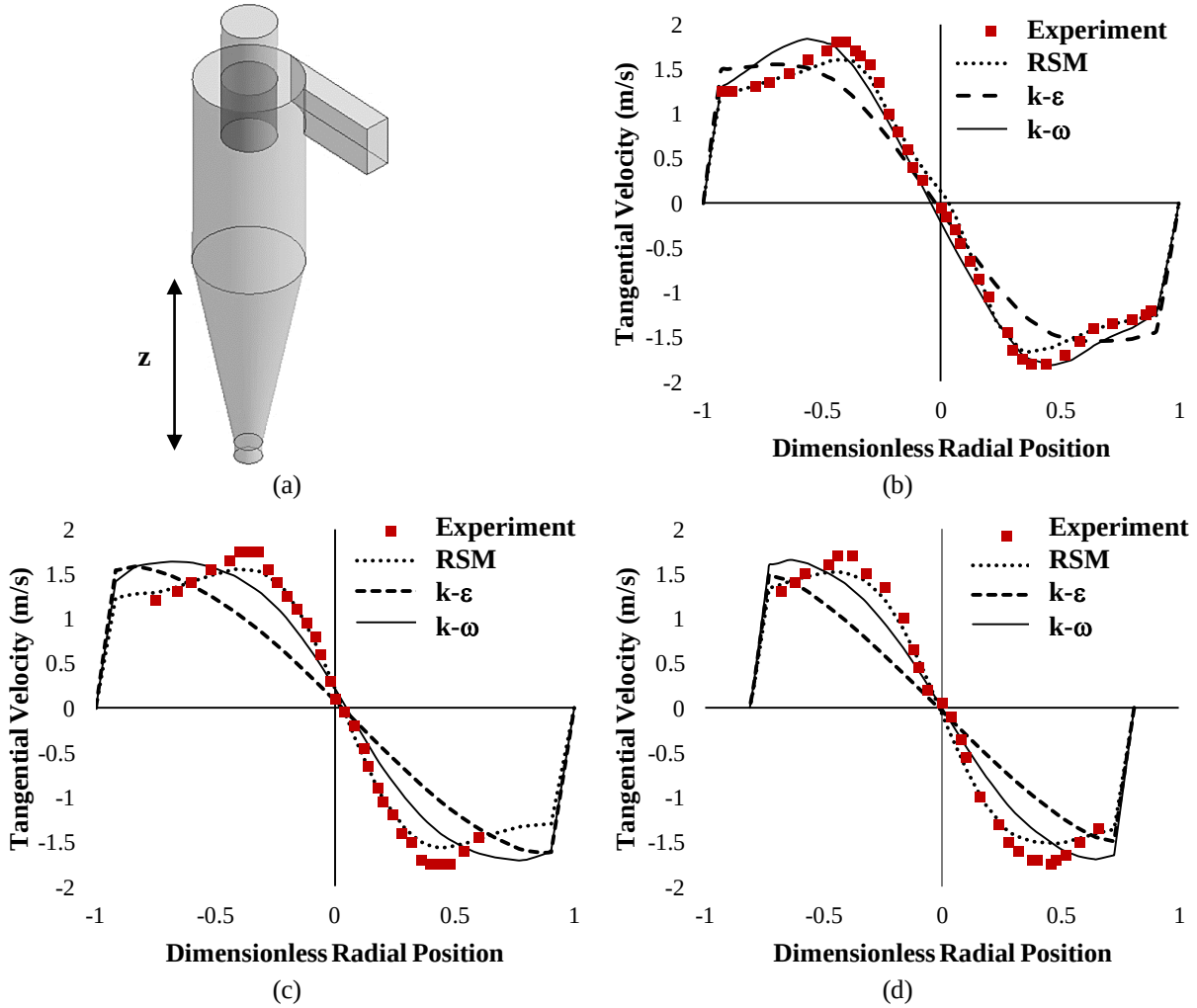

Figure 2. Tangential velocity profile at (a) z = 65 cm, (b) z = 40 cm, and (c) z = 30 cm

From the simulation results, it can be concluded that all turbulent models follow the trend of the experimental data. Basically, the k-ε and k-ω models are based on the assumption of identical values for three-dimensional fluctuation velocity which is called isotropic turbulent flow [33,59]. Hence, it is not suitable for highly laden cyclonic flows with anisotropic turbulence so those models are still not able to accurately predict the tangential flow around the vortex finder area [50,63]. The closest pattern is nominated to RSM. It then can be confidently selected to

model the multiphase turbulent flow in the suspension furnace.

The examined variable for the grid independence test using RSM is tangential velocity along the axial center inside the burner of the cylindrical suspension furnace. It is realized that finer grid impacts more accurate results but the computation demand is very intensive [39,64]. According to the results, the grid number of 1,000,000 is nominated as the most optimal grid. It is then applied to all variations of this simulation. The result is served in Figure 3.

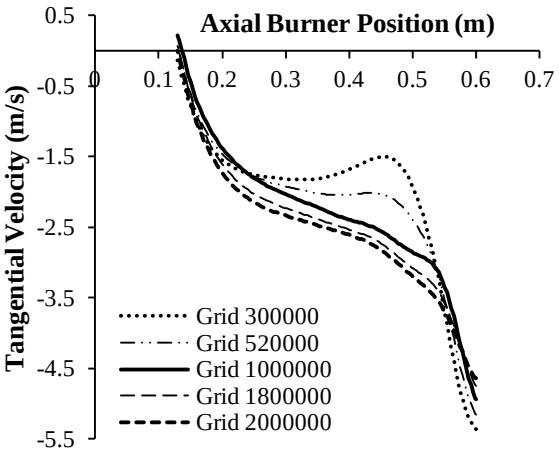

Figure 3. Grid independence test result

3.2 Flow structures under various furnace geometries and excess air amount

The section discusses the air and particle flow structures in the furnace due to the presence of 140% of excess air with the proportion of 20% axial air, 50% tangential air, and 30% secondary air. Axial air compels the rice husk to flow axially through the burner, tangential air provides a turbulent flow generator that is expected to form a swirling path in the burner, and secondary air is aimed to create the recirculating flow effect in the furnace chamber [43,65,66]. Also, the particle momentum loss is found greater under the tangential air presence which leads to a more downward movement of the particle and elongates the residence time [67].

The air flow structure in the rectangular and cylindrical furnace chambers is depicted in Figure 4. The air residence time augments due to the attendance of tangential air, 5.9 s for rectangular chamber and 9.6 s for cylindrical chamber. The longer air residence time strengthened that tangential air creates a swirl pattern that elongates the trajectories in the burner as well as in the chamber compared to axial air only [68,69]. Likewise, the air residence time in the cylindrical chamber is longer than rectangular chamber. The more intense air collision to the wall in the rectangular chamber might be the cause of the more unpatterned air pathline. Also, the figure reflects that cylindrical chamber allows air to flow smoothly in a swirl and cyclonic pathline with a less intense collision in such a way that elongates the fluid pathline in the chamber.

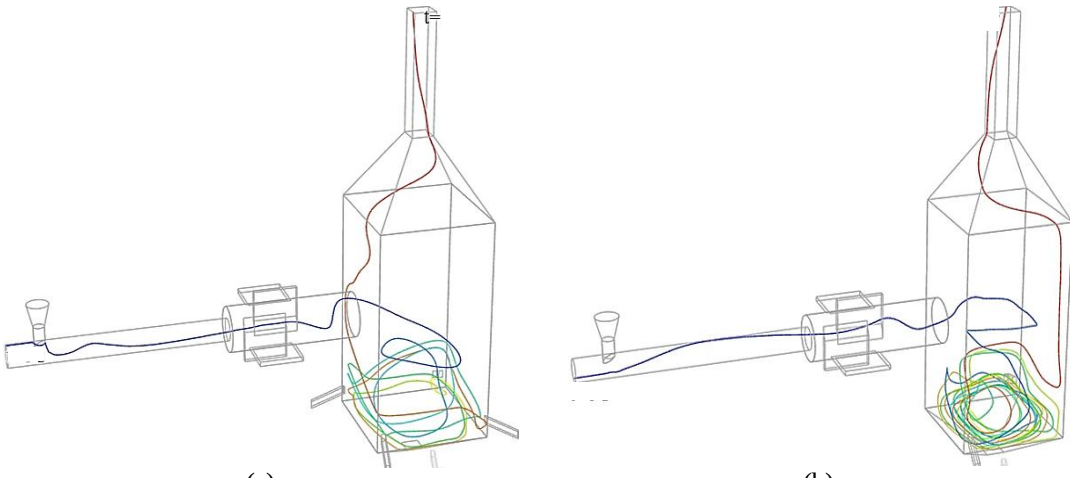

(a) (b)

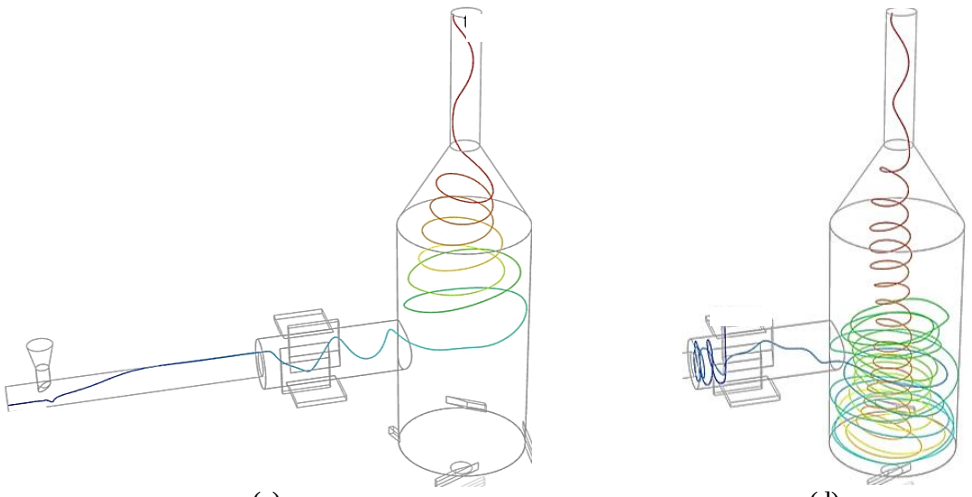

(c) (d)

Figure 4. Flow structure of air in rectangular furnace chamber (a-b) and cylindrical furnace chamber (c-d)

In some cases, the flow of rice husk particles does not coincide with the air flow because of the physicochemical properties difference between air and rice husk particle. Figure 5 informs the rice husk flow structure (in the form of particle track or trajectory) at several streams. Streams 1, 3, and 5 have residence times of 21.5 s, 22.7 s, and 18.1 s. The trajectory in stream 2 has a residence time of 5.39 s due to the particle leaving out from the outlet. Other than that, the trajectory in stream 4 occurs only in the burner. The particles do not enter the furnace due to the axial and tangential air flow collision in such a way creates a vicious recirculation flow effect. The varying observed rice husk flow structures indicate the complexity of turbulent flow whereas the data acquisition from the experiment is either difficult or expensive to be done [32,33]. Therefore, CFD simulation could be a promising solution in order to assess flow structure for industrial furnace design purposes.

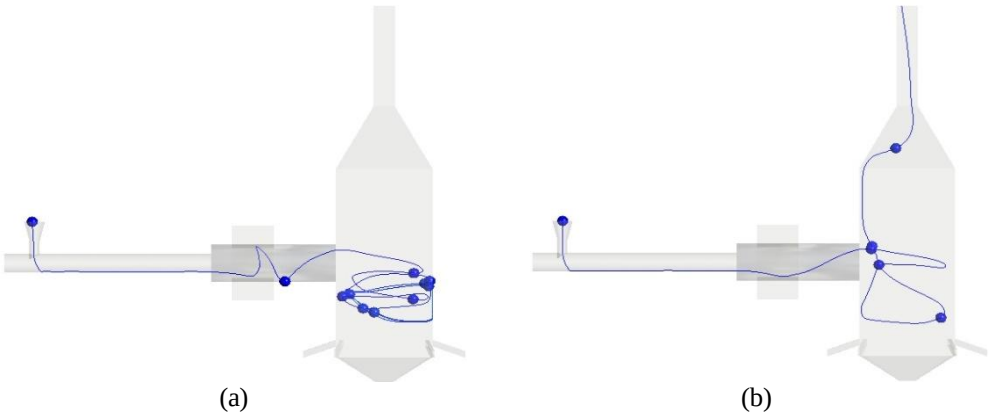

(a) (b)

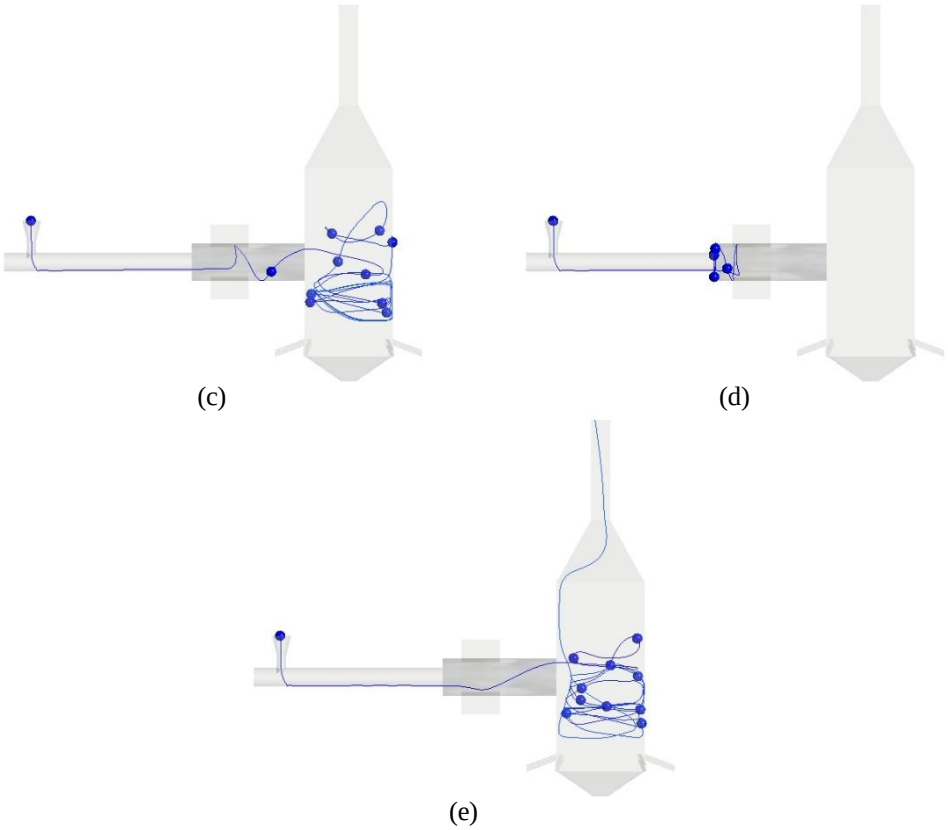

Figure 5. Rice husk particle trajectories at stream 1 (a), 2 (b), 3 (c), 4 (d), and 5 (e)

The shorter particle residence time is found in line with a larger amount of excess air from 80-200% for both furnace chamber geometries as implied in Figure 6. The particle residence time in the furnace strongly affects the degree of combustion where longer air-particle contact leads to a more complete combustion reaction [70]. Additionally, the average particle residence time for cylindrical chamber is found to be 65.2-80.5 s longer compared to rectangular chamber. Contrary to the air flow pathline, the particle track does not just go upward due to the dominance of gravitational force works on it [71]. The same phenomenon happens in cylindrical chamber where the particle flows with low intensity of collision with wall so the particle flows smoothly before it is elutriated due to the air flow field. Meanwhile, the particle flow in the rectangular chamber has a high probability of severe particle-wall collision which could drag the particle out from the furnace.

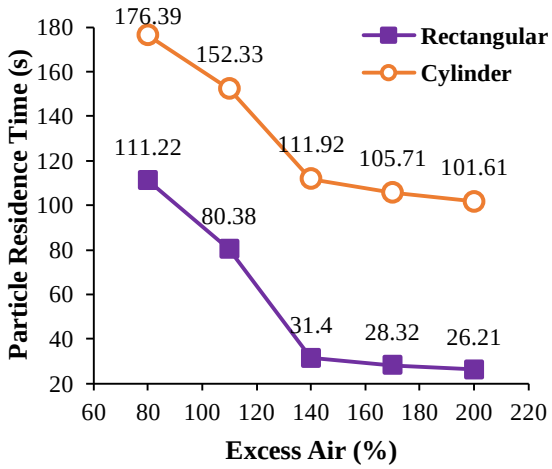

Figure 6. Particle residence time in rectangular and cylindrical chambers at various excess air amounts (fixed conditions: burner diameter = 30 cm, burner length = 60 cm, tangential air inlet angle = 90^{o})

3.3 Flow structures in rectangular furnace chamber under various burner configurations

Variations of tangential inlet angles in rectangular furnace chamber are carried out at 20 º, 45 º, 60 º, and 90 ºtowards the burner axial

position. The flow structure alteration is presented in Figures 7a-d. It can be seen that increasing the tangential air inlet angle is proven to intensify the swirl effect, augment the turbulent intensity, as well as prolong the particle residence time. The result of particle residence time and turbulence intensity is then summarized in Figure 7e. According to this figure, the most intense swirl flow occurred at a tangential inlet angle of 90 °which resulted in higher turbulent intensity (from 0.26 to 0.38%) as well as longer path length and residence time (from 2.8 to 31.4 s).

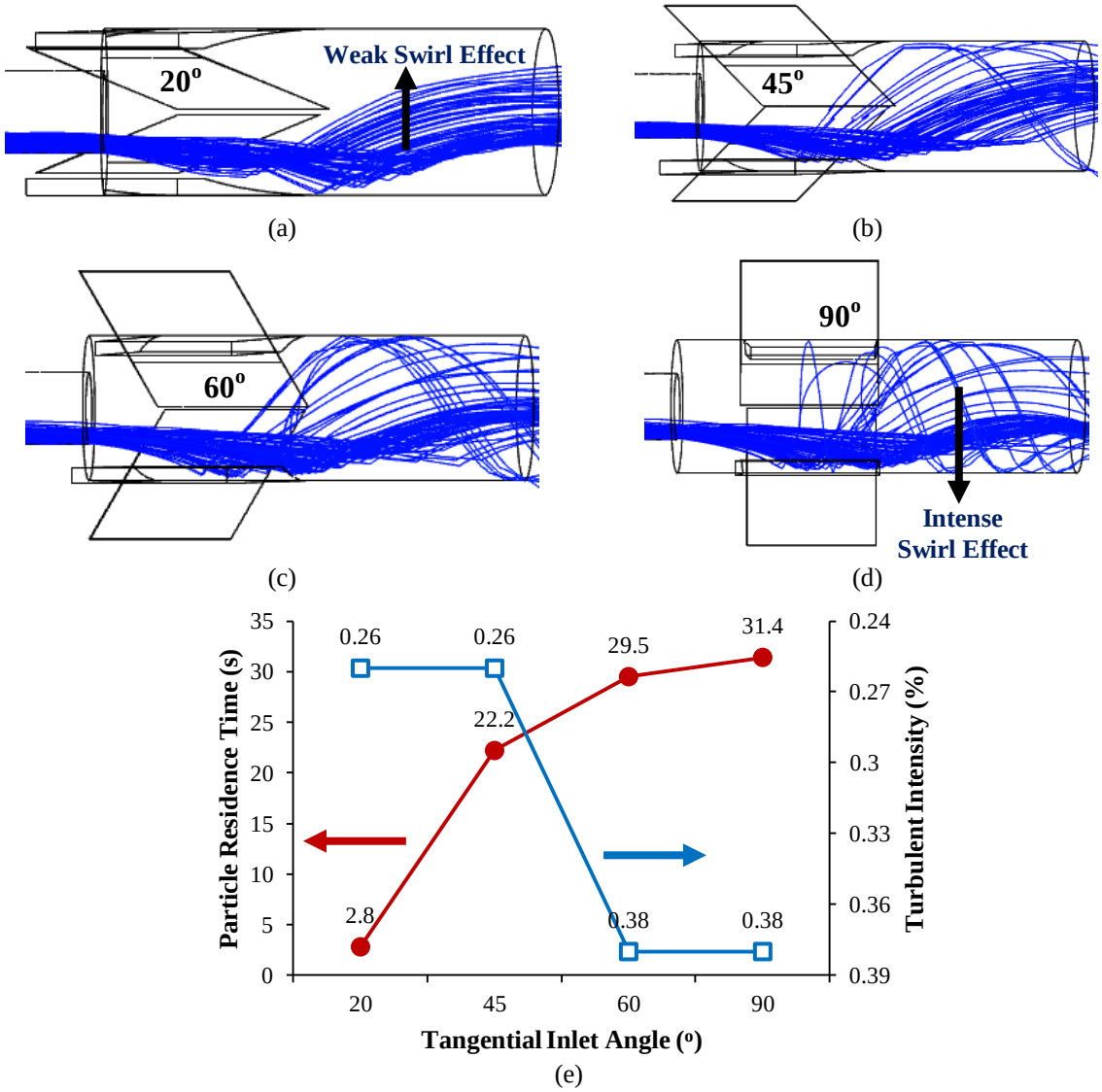

Figure 7. Flow structure in rectangular furnace chamber for burner with tangential inlet angles of 20 °(a), 45 °(b), 60 °(c), and 90 °(d); Particle residence time and turbulence intensity under various tangential inlet angles in burner (e) (fixed conditions: burner diameter = 30 cm, burner length = 60 cm, excess air amount = 140%)

The next variation lies in the burner diameter which was carried out at 30, 40, 50, and 70 cm as well as burner length at 60, 90, 120, 150, 180, and 210 cm. Figure 8 represents the opposite pattern for particle residence time under the increasing value of burner diameter and burner length. The enhancement of burner diameter alleviates the particle residence time by 1.1 s. This is also in line with the shortening of particle path length in the burner. The reason can be explained by the flow continuity principle in which the total velocity is certainly

weakening under a larger burner cross-section area due to a larger diameter [67]. Hence, the swirl effect of the particle becomes attenuating under the same value of tangential air velocity as evidenced in Figure 9.

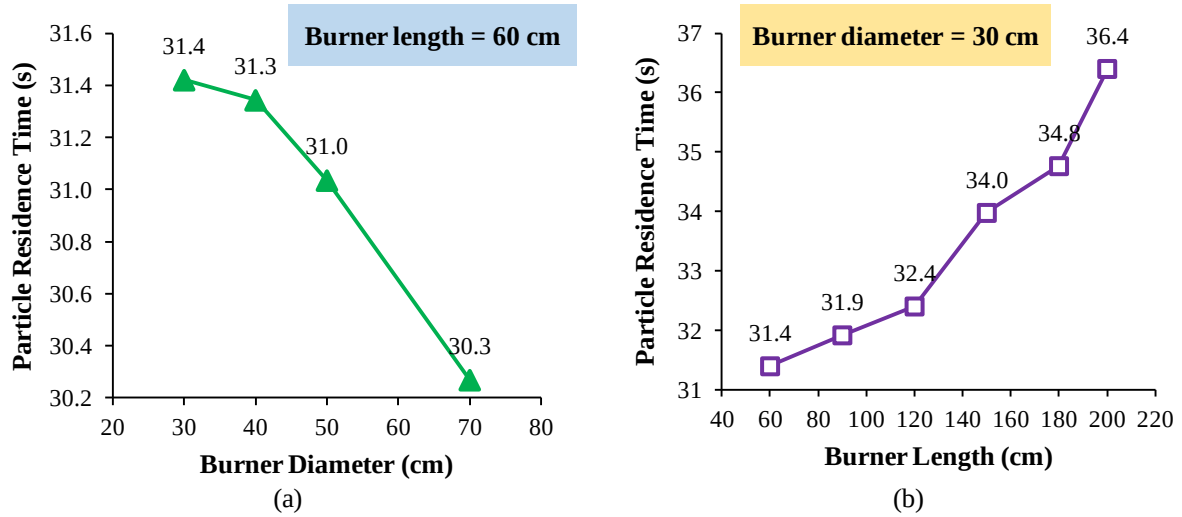

(a) (b)

Figure 8. Average rice husk particle residence time in rectangular furnace chamber under several burner diameters and lengths (fixed conditions: tangential air inlet angle = 90°, excess air amount = 140%)

In contrast, the particle residence time intensifies for 5 s along with longer burner length from 60 to 210 cm. Therefore, enlarging burner diameter for upgrading the combustion capacity must be followed by the addition of burner length as well as providing a more amount of tangential air flow rate. However, the chosen burner diameter and length for industrial furnace purposes should consider other variables such as cost of material and construction in order to meet the economic aspect [72].

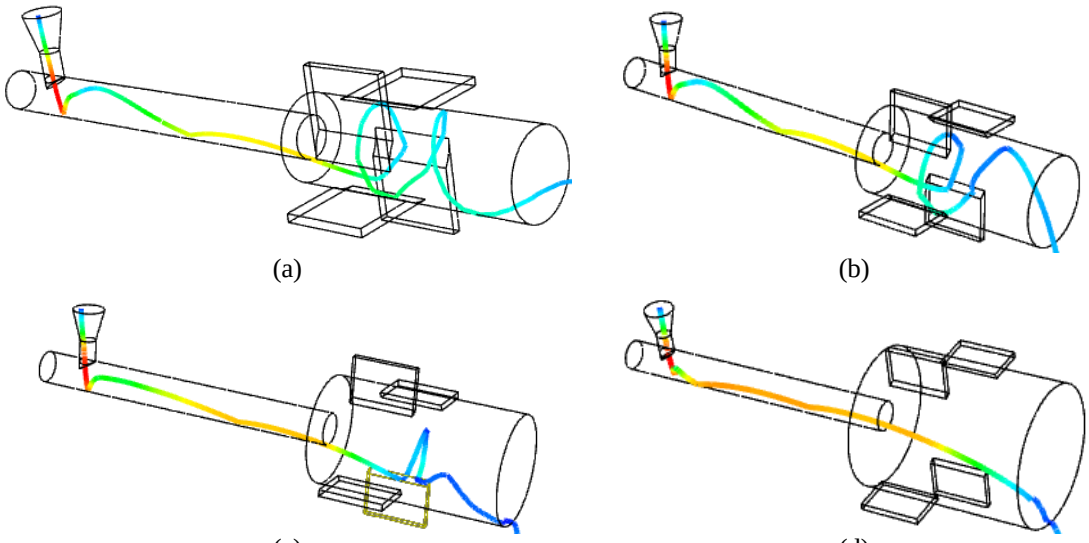

(a) (b) (c) (d)

Figure 9. Rice husk particle track in burner with diameter of 30 cm (a), 40 cm (b), 50 cm (c), and 60 cm (d)

4. Conclusions

The simulation study succeeds to investigate and intrigue the effects of furnace chamber geometry, excess air amount, burner configurations of air and rice husk cold flow structures as well as residence time in the suspension furnace. Air flows up reached to the outlet while particle flow tends to move downward due to a more significant density value. The particle-wall collision is found less intense in cylindrical chamber rather than rectangular chamber and leads to the smooth particle flow in the cylindrical chamber. As a consequence, particle residence time prolongs about 65.2-80.5 s in the cylindrical chamber. It becomes favorable for rice husk complete combustion. Instead, more amount of excess air shortens the particle residence time for both furnace chamber geometries. In addition, the burner with tangential air inlet angle of 90^{o} is proven to enhance particle residence time, increase swirl effect, and intensify turbulent intensity. Increasing burner diameter and shortening burner length also reduces the particle residence time of 1.1 s and 5 s successively. At last, the complex multiphase phenomena of air and rice husk flow structures inside the furnace chamber can be clearly expressed using CFD simulation.

Acknowledgments

The authors would thank Mr. Imam Mardhatillah Fajri (Biomass Technology Workshop ITB Jatinangor) for his kind assistance in operating ANSYS Fluent software. A great acknowledgment to Mr. Harben (Biomass Technology Workshop ITB Jatinangor) for his time to introduce and explain to us the working principle of the existing suspension biomass furnace.

References

[1] Y.W. Budhi, M. Effendy, Y. Bindar, S. Subagjo, Dynamic Behavior of Reverse Flow Reactor for Lean Methane Combustion, J. Eng. Technol. Sci. 46 (2014) 299–317. doi:10.5614/j.eng.technol.sci.2014.46.3.5.

[2] P. Hernowo, S. Steven, E. Restiawaty, A. Irawan, C.B. Rasrendra, S. Marno, Y. Meliana, Y. Bindar, Chemicals component yield prediction and kinetic parameters determination of oil palm shell pyrolysis through volatile state approach and experimental study, J. Anal. Appl. Pyrolysis. 161 (2022) 105399. doi:10.1016/j.jaap.2021.105399.

[3] Y. Bindar, S. Steven, S.W. Kresno, P. Hernowo, E. Restiawaty, R. Purwadi, T. Prakoso, Large-scale pyrolysis of oil palm frond using two-box chamber pyrolyzer for cleaner biochar production, Biomass Conv. Bioref. (2022). doi:10.1007/s13399-022-02842-1.

[4] Y. Ramli, S. Steven, E. Restiawaty, Y. Bindar, Simulation Study of Bamboo Leaves Valorization to Small-Scale Electricity and Bio-silica Using ASPEN PLUS, Bioenerg. Res. (2022) 1–9. doi:10.1007/s12155-022-10403-7.

[5] I.G. Wenten, S. Steven, A. Dwiputra, Khoiruddin, A.N. Hakim, From lab to full-scale ultrafiltration in microalgae harvesting, J. Phys.: Conf. Ser. 877 (2017) 012002. doi:10.1088/1742-6596/877/1/012002.

[6] S. Steven, D.L. Friatnasary, A.K. Wardani, K. Khoiruddin, G. Suantika, I.G. Wenten, High cell density submerged membrane photobioreactor (SMPBR) for microalgae cultivation, IOP Conf. Ser.: Earth Environ. Sci. 963 (2022) 012034. doi:10.1088/1755-1315/963/1/012034.

[7] Food and Agriculture Organizations (FAO), Country Fact Sheet on Food and Agriculture Policy Trends – Indonesia, 2017. https://www.fao.org/3/i7696e/i7696e.pdf.

[8] D.R. Panuju, K. Mizuno, B.H. Trisasongko, The dynamics of rice production in Indonesia 1961–2009, J. Saudi Soc. Agric. Sci. 12 (2013) 27–37. doi:10.1016/j.jssas.2012.05.002.

[9] S. Srinath, G.V. Reddy, Combustion and emission characteristics of rice husk in a rectangular fluidized bed combustor, 2nd International Conference on Environmental Science and Technology IPCBEE. 6 (2011) 343–346. doi:10.1016/j.chroma.2014.03.035.

[10] S. Suranani, V.R. Goli, Modeling fluidized bed combustion of rice husk, Int. Conf. Chem. Civ. Environ. Eng. (2012) 305–308.

[11] S. Steven, E. Restiawaty, Y. Bindar, Routes for energy and bio-silica production from rice husk: A comprehensive review and emerging prospect, Renew. Sustain. Energy

Rev. 149 (2021) 111329. doi:10.1016/j.rser.2021.111329.

[12] S. Azat, A. V. Korobeinyk, K. Moustakas, V.J. Inglezakis, Sustainable production of pure silica from rice husk waste in Kazakhstan, J. Clean. Prod. 217 (2019) 352–359. doi:10.1016/j.jclepro.2019.01.142.

[13] R. Blissett, R. Sommerville, N. Rowson, J. Jones, B. Laughlin, Valorisation of rice husks using a TORBED® combustion process, Fuel Process. Technol. 159 (2017) 247–255. doi:10.1016/j.fuproc.2017.01.046.

[14] I. Quispe, R. Navia, R. Kahhat, Life cycle assessment of rice husk as an energy source. A Peruvian case study, J. Clean. Prod. 209 (2019) 1235–1244. doi:10.1016/j.jclepro.2018.10.312.

[15] I. Quispe, R. Navia, R. Kahhat, Energy potential from rice husk through direct combustion and fast pyrolysis: A review, Waste Manag. 59 (2017) 200–210. doi:10.1016/j.wasman.2016.10.001.

[16] J.D. Martínez, T. Pineda, J.P. López, M. Betancur, Assessment of the rice husk lean-combustion in a bubbling fluidized bed for the production of amorphous silica-rich ash, Energy. 36 (2011) 3846–3854. doi:10.1016/j.energy.2010.07.031.

[17] D.F. Houston, Rice Chemistry and Technology, Vol. IV, 1972.

[18] S. Steven, E. Restiawaty, Y. Bindar, Simple mass transfer simulation using a single-particle heterogeneous reaction approach in rice husk combustion and rice husk ash extraction, IOP Conf. Ser.: Earth Environ. Sci. 963 (2022) 012050. doi:10.1088/1755-1315/963/1/012050.

[19] S. Steven, P. Hernowo, E. Restiawaty, A. Irawan, C.B. Rasrendra, A. Riza, Y. Bindar, Thermodynamics Simulation Performance of Rice Husk Combustion with a Realistic Decomposition Approach on the Devolatilization Stage, Waste Biomass Valor. 13 (2022) 2735–2747. doi:10.1007/s12649-021-01657-x.

[20] U. Kalapathy, A. Proctor, J. Shultz, A simple method for production of silica from rice hull ash, Bioresour. Technol. 85 (2002) 285–289. doi:10.1016/S0960-8524(02)00116-5.

[21] S. Steven, E. Restiawaty, P. Pasymi, Y. Bindar, An appropriate acid leaching sequence in rice husk ash extraction to enhance the produced green silica quality for sustainable industrial silica gel purpose, J. Taiwan Inst. Chem. Eng. 122 (2021) 51–57. doi:10.1016/j.jtice.2021.04.053.

[22] S. Steven, E. Restiawaty, P. Pasymi, Y. Bindar, Influences of pretreatment, extraction variables, and post treatment on bench-scale rice husk black ash (RHBA) processing to bio-silica, Asia-Pac. J. Chem. Eng. 16 (2021) e2694. doi:10.1002/apj.2694.

[23] S. Steven, E. Restiawaty, Y. Bindar, Operating Variables on Production of High Purity Bio-silica from Rice Hull Ash by Extraction Process, J. Eng. Technol. Sci. 54 (2022) 220304. doi:10.5614/j.eng.technol.sci.2022.54.3.4.

[24] H.B. Dizaji, T. Zeng, I. Hartmann, D. Enke, T. Schliermann, V. Lenz, M. Bidabadi, Generation of high quality biogenic silica by combustion of rice husk and rice straw combined with pre- and post-treatment strategies-A review, Appl. Sci. 9 (2019) 1–27. doi:10.3390/app9061083.

[25] R. Narvaez, R. Blanchard, A. Mena, Use of rice crops waste for energy production in Ecuador, Energy and Power. 3 (2013) 27–36. doi:10.5923/j.ep.20130303.01.

[26] R.I. Singh, A. Brink, M. Hupa, CFD modeling to study fluidized bed combustion and gasification, Appl. Therm. Eng. 52 (2013) 585–614. doi:10.1016/j.applthermaleng.2012.12.017.

[27] I.J. Fernandes, D. Calheiro, A.G. Kieling, C.A.M. Moraes, T.L.A.C. Rocha, F.A. Brehm, R.C.E. Modolo, Characterization of rice husk ash produced using different biomass combustion techniques for energy, Fuel. 165 (2016) 351–359. doi:10.1016/j.fuel.2015.10.086.

[28] J. Werther, M. Saenger, E.U. Hartge, T. Ogada, Z. Siagi, Combustion of agricultural residues, Prog. Energy Combust. Sci. 26 (2000) 1–27. doi:10.1016/S0360-1285(99)00005-2.

[29] P. Ostermeier, F. Fischer, S. Fendt, S. DeYoung, H. Spliethoff, Coarse-grained CFD-DEM simulation of biomass gasification in a fluidized bed reactor, Fuel. 255 (2019) 115790. doi:10.1016/j.fuel.2019.115790.

[30] P.N. Babaso, H. Sharanagouda, Rice husk and its applications: Review, Int. J. Curr. Microbiol. Appl. Sci. 6 (2017) 1144–1156. doi:10.20546/ijcmas.2017.610.138.

[31] V.I. Kuprianov, R. Kaewklum, K. Sirisomboon, P. Arromdee, S. Chakritthakul, Combustion and emission characteristics of a swirling fluidized-bed combustor burning moisturized rice husk, Appl. Energy. 87 (2010) 2899–2906.

doi:10.1016/j.apenergy.2009.09.009.
[32] Y. Bindar, Closing the Gaps Between Designed and Operational Unit Process Performances Using CFD Technique, in: Proceeding of The Engineering Science and Technology International Conference, Universitas Bung Hatta, Padang, 2016.
[33] Y. Bindar, Computational Engineering on Multidimensional Turbulent Flows (Rekayasa Komputasi Aliran Turbulen Multidimensi), 2017.
[34] G. Sorrentino, G. Ceriello, A. Cavaliere, M. de Joannon, R. Ragucci, Thermo-chemical manifold reduction for tabulated chemistry modeling. Temperature and dilution constraints for smooth combustion reactors, Proceedings of the Combustion Institute. 38 (2021) 5393–5402. doi:10.1016/j.proci.2020.06.144.
[35] G. Ceriello, G. Sorrentino, A. Cavaliere, P. Sabia, M. de Joannon, R. Ragucci, The role of dilution level and canonical configuration in the modeling of MILD combustion systems with internal recirculation, Fuel. 264 (2020) 116840. doi:10.1016/j.fuel.2019.116840.
[36] P. Pasymi, Y.W. Budhi, A. Irawan, Y. Bindar, Three dimensional cyclonic turbulent flow structures at various geometries, inlet-outlet orientations and operating conditions, J. Mech. Eng. Sci. 12 (2018) 4300–4328. doi:10.15282/jmes.12.4.2018.23.0369.
[37] P. Pasymi, Y.W. Budhi, Y. Bindar, Experimental and numerical investigations of fluid flow behaviors in a biomass cyclone burner, ASEAN J. Chem. Eng. 20 (2020) 88–98. doi:10.22146/ajche.56708.
[38] P. Pasymi, Y.W. Budhi, Y. Bindar, Intrinsic parameters of dry chopped miscanthus for cold particle dynamic modeling, Jurnal Teknologi. 82 (2020) 91–100. doi:10.11113/jt.v82.13534.
[39] S. Steven, E. Restiawaty, P. Pasymi, I.M. Fajri, Y. Bindar, Digitalized turbulent behaviors of air and rice husk flow in a vertical suspension furnace from computational fluid dynamics simulation, Asia-Pac. J. Chem. Eng. (2022). doi:10.1002/apj.2805.
[40] N. Sylvia, R. Mutia, Malasari, R. Dewi, Y. Bindar, Yunardi, A Computational Fluid Dynamic Comparative Study on CO2 Adsorption Performance using Activated Carbon and Zeolite in a Fixed Bed Reactor, IOP Conf. Ser:. Mater. Sci. Eng. 536 (2019) 012042. doi:10.1088/1757-899X/536/1/012042.
[41] N. Malekjani, S.M. Jafari, Simulation of food drying processes by Computational Fluid Dynamics (CFD); recent advances and approaches, Trends Food Sci. Technol. 78 (2018) 206–223. doi:10.1016/j.tifs.2018.06.006.
[42] M. Nakhaei, B. Lu, Y. Tian, W. Wang, K. Dam-Johansen, H. Wu, CFD modeling of gas-solid cyclone separators at ambient and elevated temperatures, Processes. 8 (2020) 1–26. doi:10.3390/pr8020228.
[43] M. Rozainee, S.P. Ngo, A.A. Salema, K.G. Tan, Computational fluid dynamics modeling of rice husk combustion in a fluidised bed combustor, Powder Technol. 203 (2010) 331–347. doi:10.1016/j.powtec.2010.05.026.
[44] Y. Wang, L. Yan, CFD studies on biomass thermochemical conversion, Int. J. Mol. Sci. 9 (2008) 1108–1130. doi:10.3390/ijms9061108.
[45] J. Konttinen, S. Kallio, M. Hupa, F. Winter, NO formation tendency characterization for solid fuels in fluidized beds, Fuel. 108 (2013) 238–246. doi:10.1016/j.fuel.2013.02.011.
[46] A. Gungor, Simulation of emission performance and combustion efficiency in biomass fired circulating fluidized bed combustors, Biomass Bioenergy. 34 (2010) 506–514. doi:10.1016/j.biombioe.2009.12.016.
[47] L. Chanphavong, K.A. Al-Attab, Z.A. Zainal, Flameless Combustion Characteristics of Producer Gas Premixed Charge in a Cyclone Combustor, Flow, Turbul. Combust. (2019).
[48] R. Panneerselvam, S. Savithri, G.D. Surender, CFD simulation of hydrodynamics of gas-liquid-solid fluidised bed reactor, Chem. Eng. Sci. 64 (2009) 1119–1135. doi:10.1016/j.ces.2008.10.052.
[49] J. Chen, B. Haynes, D. Fletcher, A numerical and experimental study of tangentially injected swirling flow, 2nd International Conference on CFD in the Minerals and Process Industries. (1999) 485–490.
[50] M. Dohnal, J. Hájek, Computational analysis of swirling pipe flow, Chem. Eng. Trans. 52 (2016) 757–762. doi:10.3303/CET1652127.
[51] C.C. Shweta, J.H. Bhangale, K.R. Sonawne, CFD analysis for investigation of design parameter of cyclone separator, Int. J. Eng. Dev. Res. 7 (2019) 461–467.

[52] M. Azadi, M. Azadi, A. Mohebbi, A CFD study of the effect of cyclone size on its performance parameters, J. Hazard. Mater. 182 (2010) 835–841. doi:10.1016/j.jhazmat.2010.06.115.

[53] P. Pasymi, Y.W. Budhi, Y. Bindar, The effect of inlet aspect ratio (RIA) to the three dimensional mixing characteristics in tangential burner, ARPN J. Eng. Appl. Sci. 12 (2017) 5300–5306.

[54] C.B. Dinh, C.C. Liao, S.S. Hsiau, Numerical study of hydrodynamics with surface heat transfer in a bubbling fluidized-bed reactor applied to fast pyrolysis of rice husk, Adv. Powder Technol. 28 (2017) 419–429. doi:10.1016/j.apt.2016.10.013.

[55] S. Yang, L. Peng, W. Liu, H. Zhao, X. Lv, H. Li, Q. Zhu, Simulation of hydrodynamics in gas-solid bubbling fluidized bed with louver baffles in three dimensions, Powder Technol. 296 (2016) 37–44. doi:10.1016/j.powtec.2015.09.026.

[56] M.R. Khosravi Nikou, M.R. Ehsani, Turbulence models application on CFD simulation of hydrodynamics, heat and mass transfer in a structured packing, Int. Commun. Heat Mass Transf. 35 (2008) 1211–1219. doi:10.1016/j.icheatmasstransfer.2008.05.017.

[57] A. Gungor, U. Yildirim, Two dimensional numerical computation of a circulating fluidized bed biomass gasifier, Comput. Chem. Eng. 48 (2013) 234–250. doi:10.1016/j.compchemeng.2012.09.012.

[58] S. Demir, A. Karadeniz, M. Aksel, Effects of cylindrical and conical heights on pressure and velocity fields in cyclones, Powder Technol. 295 (2016) 209–217. doi:10.1016/j.powtec.2016.03.049.

[59] ANSYS, ANSYS Fluent Theory Guide 2019 R3, 2019.

[60] M.L. Corradini, C. Zhu, L.-S. Fan, R.-H. Jean, Multiphase Flow, in: Handbook of Fluid Dynamics, Second Edition, Cambridge University Press, 2016: pp. 1–92.

[61] M. Mandø, L. Rosendahl, On the motion of non-spherical particles at high Reynolds number, Powder Technol. 202 (2010) 1–13. doi:10.1016/j.powtec.2010.05.001.

[62] A. Haider, O. Levenspiel, Drag coefficient and terminal velocity of spherical and nonspherical particles, Powder Technol. 58 (1989) 63–70. doi:10.1016/0032-5910(89)80008-7.

[63] A.J. Hoekstra, J.J. Derksen, H.E.A. Van Den Akker, An experimental and numerical study of turbulent swirling flow in gas cyclones, Chem. Eng. Sci. 54 (1999) 2055–2065. doi:10.1016/S0009-2509(98)00373-X.

[64] S. Yang, H. Wang, Y. Wei, J. Hu, J.W. Chew, Particle-scale characteristics of the three distinct regions in the multi-chamber slot-rectangular spouted bed, Powder Technol. 360 (2020) 658–672. doi:10.1016/j.powtec.2019.10.038.

[65] M. Koksal, Gas mixing and flow dynamics in circulating fluidized beds with secondary air injection, 2001.

[66] L.E. Ersoy, M. Koksal, F. Hamdullahpur, Effects of mode of secondary air injection on gas and solid velocity profiles in a CFB riser, in: Circ. Fluid. Bed Technol. VI, 1999: pp. 417–422.

[67] C.J. Geankoplis, Principles of Momentum Transfer and Applications, in: Transport Processes and Unit Operations, Third Edition, 1993: pp. 114–118.

[68] S. Nemoda, V. Bakić, S. Oka, G. Zivković, N. Crnomarković, Experimental and numerical investigation of gaseous fuel combustion in swirl chamber, Int. J. Heat Mass Transf. 48 (2005) 4623–4632. doi:10.1016/j.ijheatmasstransfer.2005.04.004.

[69] L. V. Ziqiang, L. Guangqiang, L. Yingjie, Optimization study on bias angle of a swirl burner with tangential inlet air, Int. J. Smart Home. 10 (2016) 171–180. doi:10.14257/ijsh.2016.10.3.17.

[70] M. Rozainee, Production of amorphous silica from rice husk in fluidised bed system, 2007.

[71] P.A. Funk, K.D. Baker, Dust cyclone technology - A literature review, J. Cotton Sci. 17 (2013) 40–51.

[72] R. Turton, R.C. Bailie, W.B. Witing, J.A. Shaeiwitz, Profitability Analysis, in: Analysis, Synthesis, and Design of Chemical Processes, Third Edition, Pearson Education, Inc., 2009: pp. 297–360.